IEEE Access
Multidisciplinary ⋮ Rapid Review ⋮ Open Access Journal

Received August 27, 2021, accepted September 6, 2021, date of publication September 10, 2021,
date of current version September 20, 2021.

Digital Object Identifier 10.1109/ACCESS.2021.3111964

Proactive Power Control and Position Deployment for Drone Small Cells: Joint Supervised and Unsupervised Learning

SHAO-HUNG CHENG, (Member, IEEE), YEN-TING SHIH, AND KO-CHIN CHANG, (Member, IEEE)
Electrical and Electronic Engineering Department, Chung Cheng Institute of Technology, National Defense University, Taoyuan 335, Taiwan
Corresponding author: Shao-Hung Cheng (locoling@gmail.com)

This work was supported by the Ministry of Science and Technology (MOST) of Taiwan under grant MOST 108-2218-E-606-003-MY2 and grant MOST 110-2221-E-606-010-.

ABSTRACT Since unmanned aerial vehicles (UAV) are easily deployed, highly mobile, and hover capability, they are utilized for many commercial applications. In particular, small cells mounted on UAVs, also known as drone small cells (DSC), may provide temporary relief or ancillary programs for the wireless network. In this paper, we design a prediction-based proactive drone management (P^2DM) framework to reduce network interference and improve energy efficiency in the multiple DSCs scenario. The P^2DM framework can be divided into offline and online phases. In the offline phase, supervised learning is used to build a highly accurate mobility prediction model according to the historical data. The prediction model is launched in the online phase to predict the user position only using a small sample set. The system proactively determines whether a DSC should be awake or asleep at the next timeslot due to the predicted user positions. Since DSC has more longer awake time in the deep sleeping mode, it is previously awoken to avoid data propagation delay. To further overcome the difficulty of obtaining the key performance indicator data (i.e., labeled data) in the online phase, an unsupervised learning technique is employed for DSC repositioning and power control to improve energy efficiency. Our simulation results show that the P^2DM framework can demonstrate the advantage in terms of execution time and energy efficiency compared to the existing method based on genetic algorithm (i.e., a heuristic algorithm).

INDEX TERMS Data driven, supervised learning, unsupervised learning, mobility prediction, drone small cells.

I. INTRODUCTION

Unmanned aerial vehicles (UAV), also known as drones, can serve as aerial small cells to improve service coverage for enhanced wireless network capacity due to flexible motility [1]. This will enable visual line-of-sight (LoS) communications and open many emerging services [2]. Indeed, the drone small cells (DSCs) can deliver disaster recovery and temporary networking and can follow a group of users assuring service continuity [3]. Notably, artificial intelligence (AI) has been considered as a key enabling technology for beyond 5G wireless networks integrated with Drones. AI-based methods act as powerful tools to promote highly dynamic DSCs communication networks [4]. Hence, there is a growing commercial interest in integrating DSCs and AI into the wireless mobile network ecosystem.

The associate editor coordinating the review of this manuscript and approving it for publication was Ding Xu.

A. MOTIVATION

Single DSC has limited power capacity, payload capacity, and flight time, whereas a group of DSCs can be coordinated to provide better quality-of-service (QoS) levels [5]. However, there are still several challenges that must be overcome. 1) Since DSCs and users are both mobile, the corresponding wireless network scenarios are intrinsically dynamic and complex. Hence, it isn't easy to build optimization models via current techniques or experts' experience in such networks. 2) To conserve frequency band resources, DSCs will use the same frequency band. This could lead to interference in user

devices that are served by multiple DSCs. The interference becomes particularly severe when the DSCs are close to each other. 3) DSCs can only carry a limited number of batteries, and flight time is shortened if communication devices share a drone's battery. Therefore, energy efficiency is an important problem for DSCs.

If the DSC does not serve any served users, it can reduce energy consumption and extend the flight time by switching to sleeping mode. When more components of a DSC have turned off, the DSC has less energy consumption. But, this increases the time needed to wake the DSC. Before mobile users begin to request data, we expect a sleeping DSC to be proactively woken up based on the mobility prediction model. This can achieve significant amounts of energy saving without additional delays. According to a small amount of input data, the accurate prediction of mobile users is a challenging problem.

In recent years, some data-driven solutions for complex telecommunication problems have been suggested in the literature. Hence, machine learning is now rapidly being applied to communication networks [6]. The most commonly used machine learning methods may be broadly categorized as supervised learning (SL), unsupervised learning (UL), and reinforcement learning (RL) [7].

1) In the SL approach, labeled historical data are analyzed to construct prediction or classification models suitable for practical application. If labeled data correspond to key performance indicators (KPIs) (e.g., system throughput), the labeled data must be obtained by collecting data from real operational networks over a sufficiently long time or simulating the data. In our previous work [8], a data-driven biadaptive self-organizing network (Bi-SON) framework based on a SL technique was developed to improve energy efficiency for ultra-dense small cells. It assumes that the labeled throughput data is available. Also, the training process and updating process of data-driven models spend a certain amount of execution time.
2) In the UL approach, the hidden structures can be found from the unlabeled data. It can save the time of collecting labeled data and the training time. Our previous work [9] compared the proposed affinity propagation power control (APPC) mechanism based on an UL technique with the data-driven Bi-SON framework based on a SL technique. The energy efficiency of small cell networks in the APPC mechanism is similar to that in the Bi-SON framework. Because the UL approach does not require any labeled data, it is unnecessary to collect real data or perform simulation, which easier to implement the temporary dispatched DSC networks. Our previous work [10], [11] proposed an UL approach to reduce interference for the temporary and dynamic drone base stations (i.e., an instant network topology).
3) In the RL approach, each action is matched to a corresponding reward, and the system learns the optimal actions that lead to the greatest accumulation of rewards. [12] devised a double deep Q-network-based resource allocation method that minimizes the total power consumption subject to the constraints on the transmit power of each remote radio head (RRH) and user rates in the cloud radio access network. [13] is an extension of [12] which focuses on energy efficiency maximization instead of power minimization. In the offline stage, the RL agent calculates the reward by combining the user satisfaction (i.e., greater than or equal to the target data rate of the user) and power saving of all RRH in a centralized manner. The user data rate may be reported from a pre-built cloud radio access network or be obtained from simulation.

According to different network scenarios, a suitable solution may be selected by analyzing the network's optimization targets and the characteristic of its data.

B. CONTRIBUTIONS

In this paper, we propose a prediction-based proactive drone management (P^2DM) framework to mitigate interference and increase energy efficiency in DSC networks. The P^2DM framework utilities the SL techniques in the offline stage and the UL techniques in the online stage to improve system performance without setting up real DSC networks or performing simulation previously. The contributions of this paper are described as follows:

1) The P^2DM framework is proposed to enhance the energy efficiency of moving group users and DSCs. Compared with the baseline scheme, the proposed mechanism can improve that by 133.9%.
2) The random forest (RF) is one of the SL techniques used to predict and estimate users' location by analyzing the historical position data. These data are collected by the original macro cell in the service area. According to the mobility prediction model using a small amount of input data, each DSC's operating parameters can be proactively determined in advance.
3) The K-means clustering (KMC) is one of the UL techniques applied to find the hidden cluster structures via the input data of user location information predicted by RF. In the cluster structures, the found cluster centers are used as candidate positions of the adjacent DSCs, and our algorithm further performs power control to reduce interference and save energy.
4) The UL of the proposed P^2DM in operation does not require any labeled data. Because of this, we need not collect the labeled data from real operational DSC networks over a sufficiently long time or perform the simulation to obtain the data. The advantage of P^2DM with the KMC in terms of execution time is demonstrated.

C. ORGANIZATION

The remainder of this article is organized as follows. A literature review is presented in Section II. Section III details

the system architecture, channel model, and KPIs of the DSC networks. The P^{2}DM framework and its important algorithms are described in Sections IV and V, respectively. An assessment of the P^{2}DM framework's performance is provided in Section VI. Finally, Section VII concludes the paper.

II. RELATED WORK

Table 1 summarizes the mobility prediction of user and energy efficiency improvement of small cells according to the following conditions: 1) Prediction of mobile users; 2) Placement of DSCs; 3) Deep sleep of small cell; 4) Energy efficiency; and 5) Multiple DSCs. In this paper, our primary objectives are the resource allocation of small cells and the reposition of drones via mobile users' mobility prediction. In the literature, [14]–[17] discussed the prediction model for mobile users. In [14], the use of support vector machines (SVMs) was proposed to predict the mobile users' movements over short time scales in highly dynamic ultra-dense small cell networks with frequently switching users. This approach allowed for real-time position predictions without invoking a high data collection load. However, the authors of [14] only provided the concepts and process flow of this method without providing experimental evidence to prove their efficacy. [15] proposed a Spatio-temporal location prediction model based on Long Short-Term Memory (LSTM) model for mobile users. LSTM was an artificial recurrent neural network (RNN) architecture used in the field of deep learning. The prediction model can predict the user's location at the next timeslot, and then the edge server can preload the user's requirement and enhance the quality of experience. In [16], the authors proposed a novel deep learning-based predictive beamforming scheme in the presence of UAV jittering. In particular, the altitude angle between the UAV and the user at the current timeslot was predicted using the angle estimates in the previous slots. Simulation results showed that the proposed scheme could accurately track the variation of the angles. In [17], machine learning techniques are utilized to learn mobile users' mobility and predict their moving directions. By tracking users' trajectories, the authors brought out the beam tracking methods based on users' mobility. The learned deep neural network was used to predict the user's trajectory with up to 80 percent prediction accuracy. The authors of [18] evaluated the accuracy of many classifiers using 121 datasets of the University of California (UCI) Machine Learning Repository. They concluded that the best classifier was the RF, followed by the SVM and neural networks. However, the RF was not utilized to predict the location of mobile users in the literature.

In [19]–[23], the authors proposed to update the position of UAVs for enhancing the KPI of the wireless networks. In [19], the authors proposed a novel Quality-of-Experience-driven UAV-assisted communications framework, which uses the mean opinion score (MOS) to assess user satisfaction. In this framework, Q-learning is used to solve UAV positions and dynamic movements that maximize the MOS. In [20], the authors focused on investigating the performance of two UAV selection strategies and maximizing the throughput of the network. Further, an algorithm was proposed to find the optimal position/coordinates of the selected UAV. In [21], the UAVs' location planning problem was investigated based on the RL algorithm. By deploying multiple UAVs in suitable locations, the communication services can meet different users' different requirements. In [22], the authors studied the joint optimization of UAVs' 3D placement and resource allocation in a multi-UAV system. Numerical results show that the proposed algorithm maximizes the minimum achievable expected rate with low complexity. In [23], the author investigated a multi-UAV-aided relaying network to maximize the minimum rate by optimizing the UAVs' positions and resource allocations.

TABLE 1. Summary of mobility prediction of user and energy efficiency improvement of small cells.

Reference	Research Category
[14]–[18], [25]	Prediction of mobile user
[19]–[23]	Placement of drone small cells (DSCs)
[24], [25]	Deep sleep of small cell
[19], [24]–[29]	Energy efficiency
[19], [20], [22], [23], [26], [27]	Multiple drone small cells (DSCs)

On the other hand, in [24]–[27], the authors considered the power control of small cells to improve energy efficiency. In [24], sleeping strategies for small cells were investigated by switching off certain hardware modules to reduce power consumption without degrading the QoS. The power-saving modes of small cells were categorized by sleeping depth. In stand-by sleeping mode (i.e., the light sleeping depth), the small cell only turns off its radio frequency components and power amplifier (PA) so that it can be woken up very quickly. The small cell further turns off the baseband (BB) component in the deep sleeping mode while its power source and back-end connections are the only active hardware modules. Hence, the deep sleeping DSC needs to take a longer wake up to switch the active mode. In the passive cell ON/OFF process, the awakening time required for the cell could cause additional data propagation delay between the cell and the user. In [25], the stand-by and deep stages for sleep mode were also considered. The authors proposed a novel sleep mode optimization approach to minimize the power consumption while the arriving user traffic is sufficiently covered. In [26], a noncooperative game was used to model the relationship between LoS links, energy management, and the optimal 3D location of each UAV for improving the downlink coverage and energy efficiency of multi-UAV networks. This approach allows UAVs to update their network scheduling schemes and resource allocation strategies dynamically. In [27], a learning-based approach was developed to solve the energy efficiency problem. The trajectories and transmission powers of the UAVs were determined by a multi-agent Q-learning-based trajectory-acquisition and power-control algorithm. The energy efficiency maximization problems in small cells' communication

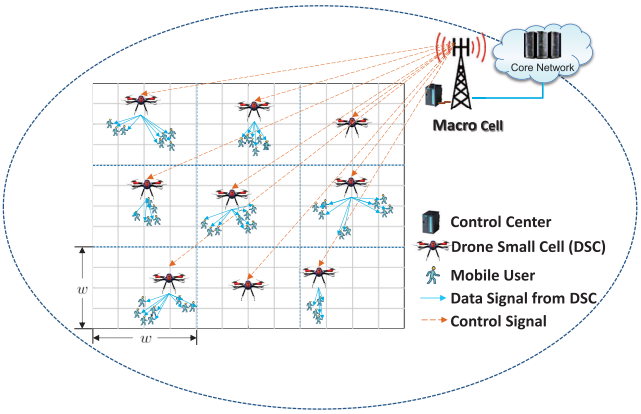

FIGURE 1. The dorn small cell (DSC) architecture.

services have been well studied in [24]–[27], where the computing process was not considered. [28], [29] applied the computation energy efficiency, which additionally considered the number of computation bits performed by the user and the user's total consumed energy in the process of local calculation.

Although the abovementioned studies have contributed significantly to the optimization of UAV-enabled wireless networks [16], [19]–[23], [26], [27], [29], dynamic group user movement prediction, multi-DSC sleep-mode power consumption control, DSC repositioning, and simple machine learning techniques were not utilized simultaneously to improve energy efficiency.

III. SYSTEM MODEL

A. SYSTEM ARCHITECTURE

Fig. 1 illustrates the system architecture in this study. The service coverage zone in a macro cell is presumed to be rectangular in shape and divisible into N small areas. One small area is w(m) $\times$ w(m). Each small area may be further divided into $F \times F$ small grids. Each small area is assumed to be serviced by only one DSC. Each DSC will only fly within its small area, which prevents DSCs from colliding with each other. The N DSCs fly at a fixed altitude of h, and the horizontal coordinates of the $n \in N$ DSCs are $D_n = [x_n, y_n] \in \mathbb{R}^2$. The system environment has K users, and the dynamic horizontal coordinates of the k-th user are $M_k = [x_k, y_k] \in \mathbb{R}^2$.

The access links of N DSCs are all set as the same frequency band f_{AL}. Hence, the users may be interfered with by the unserved DSCs. Each DSC/user has only one omnidirectional antenna. Each user only is served by one DSC. The backhaul links between the macro cell and DSCs use the frequency band f_{BL} that is different from f_{AL}. Therefore, the interference from the macro cell is negligible. Optical fibers connect the macro cell to the core network. The reported data from the DSCs are collected and analyzed by an edge control center in the macro cell. Then the control center makes decisions about the DSCs' operating parameters after analyzing these data.

B. USER MOBILITY MODEL

We create our user mobility dataset from simulated data. In real life, mobile users are often involved in team activities. The reference point group mobility (RPGM) model is one of the most commonly used group mobility for mobile networks [30]. In a group, each user follows a group leader that determines the group's motion behavior. The random waypoint mobility model generates the predefined paths of group leaders [31]. The group members in a group are usually randomly distributed around the group leader. Equation (1) determines how much the motion of group members deviates from their group leader as follows [32]:

$$\begin{cases} |v^t_{member}| = random(-1, 1) \cdot \eta_s \cdot v_{max} + |v^t_{leader}| \\ \theta^t_{member} = random(-1, 1) \cdot \eta_a \cdot \theta_{max} + \theta^t_{leader}, \end{cases} \tag{1}$$

where θ_{max} is the maximum shift angle of each user and V_{max} is the maximum moving speed of each user. Thus, the moving speed of each user varies over time (i.e., not a fixed value). Denote η_s and η_a as the speed deviation factor and the angle deviation factor, respectively, where $0 < \eta_s < 1$, and $0 < \eta_a < 1$. Based on the group leader, η_s and η_a are used to control the deviation of the velocity (magnitude and direction) of group members. The total number of users in the user mobility dataset equals the sum of group members in each group leader.

C. RADIO PROPAGATION MODEL

Unlike terrestrial base stations, DSCs can provide LoS communication links to users on the ground. The radio propagation model is used to model the downlink transmission from a DSC to a user and is commonly modeled by considering the LoS and Non-line-of-sight (NLoS) signals and their probabilities separately [33]. Considering the free space propagation loss, the channel model [34] of the air-to-ground link is expressed as follows:

$$L^{\varphi}_{n,k} = 20\log(\frac{4\pi f_{AL} d_{n,k}}{c}) + \delta_{\varphi}(\text{dB}), \quad \varphi \in \{\text{LoS,NLoS}\}, \tag{2}$$

where c is the speed of light, δ_{φ} is the mean additional losses for link, and $\varphi \in \{\text{LoS,NLoS}\}$ indicates the LoS and NLoS cases, respectively. The euclidean distance between DSC n and user k is $d_{n,k} = \sqrt{h^2 + (M_k - D_n)^2}$.

To characterize the random effect of LoS and NLoS channel for the air-to-ground link [35], the probabilities of LoS for a user k associated with DSC n is

$$P^{LoS}_{n,k} = \frac{1}{1 + \tau_1 \exp(-\tau_2[\theta_{n,k} - \tau_1])}, \tag{3}$$

where $\theta_{n,k} = \arctan(\frac{h}{r_{n,k}})$ is the elevation angle and $r_{n,k} = \sqrt{(x_k - x_n)^2 + (y_k - y_n)^2}$ is the horizontal distance between the DSC n and user k. By definition, the NLoS probability is expressed as $P^{\text{NLoS}}_{n,k} = 1 - P^{LoS}_{n,k}$. Then, the average path-loss

for the link $L_{n,k}$ can be written as

$$L_{n,k} = \sum_{\varphi\in\{\text{LoS,NLoS}\}} P_{\varphi} L_{n,k}^{\varphi} = \frac{\delta_{LoS} - \delta_{\text{NL}oS}}{1+\tau_1 \exp(-\tau_2[\theta_{n,k}-\tau_1])} + 20\log(\frac{r_{n,k}}{\cos(\theta_{n.k})}) + 20\log(\frac{4\pi f_{AL}}{c}) + \delta_{\text{NL}oS}. \quad (4)$$

Let P_n^{tra} denote the transmission power of DSC n. In addition, P_{max}^{tra} is the maximum transmission power of a DSC. The received signal power of user k from DSC n is given by

$$P_{n,k}^{rec} = P_n^{tra}(10^{L_{n,k}/10})^{-1}. \quad (5)$$

D. SYSTEM THROUGHPUT

In the downlink of the DSC networks, the signal-to-interference-plus-noise-ratio $\zeta_{n,k}$ from DSC n to user k can be expressed as

$$\zeta_{n,k} = \frac{P_{n,k}^{rec}}{B_{n,k}N_0 + \sum_{l\neq n}^{N} P_{l,k}^{rec}}, \quad (6)$$

where $P_{l,k}^{rec}$ is the strength of the interference signal from DSC l to user k and N_0 is the power spectral density of additive white Gaussian noise. $B_{n,k}$ is the bandwidth allocated to the downlink between DSC n and user k. We assume $B_{n,k} = B/|\mathbf{U}_n|$ based on the bandwidth allocations are performed in full-buffer mode. The available bandwidth of each DSC is B, the set of users served by DSC n is $\mathbf{U}_n$, and the number of users in DSC n is $|\mathbf{U}_n|$. The total system throughput of the DSC networks Υ_{sum} is expressed as

$$\Upsilon_{sum} = \sum_{n}^{N}\sum_{k}^{K} r_{n,k} = \sum_{n}^{N}\sum_{k}^{K} B_{n,k} log_2(1+\zeta_{n,k}), \quad (7)$$

where the throughput $r_{n,k}$ of user k from DSC n.

E. POWER CONSUMPTION

The energy consumption of a small cell comes from its PA, BB engine, radio frequency small-signal transceiver, direct current (DC) converter, and main supply (MS) [36], [37]. It is assumed that the operating modes of each DSC n include the "active," "stand-by sleeping," "deep sleeping," and "off" modes. The number of components turned off in each mode is different. All of the components are turned off in the off mode, resulting in zero energy consumption. All of the components are turned on in the active mode. The power consumption of DSC n in the active mode P_n^{ACT} is given by [38]

$$P_n^{ACT} = \frac{\iota_n P_{PA,max} + N_{ant}\frac{B}{10[\text{MHz}]}[P_{RA}+P_{BB}]}{(1-\sigma_{DC})(1-\sigma_{MS})}, \quad (8)$$

where P_{RA} and P_{BB} denote the radio frequency and BB base power consumptions (i.e., using one antenna and 10 MHz) while $P_{PA,max}$ is the PA maximum transmission power. σ_{DC} and σ_{MS} denote the loss factors of the different components. N_{ant} is set to 1 based on each DSC has only one omnidirectional antenna. We adopt the full-buffer traffic model [39], i.e., the cell load of $\iota_n = 1$. Each small cell has two sleep states, namely stand-by and deep sleeping [40]. The stand-by model consumes higher power but is faster to wake up compared to the deep sleeping model. In the case of stand-by sleeping mode, since the BB component is ON during the sleep period, wake-up time is shorter than in the deep sleeping model [41]. Based on the PA and radio frequency components are turned off in the stand-by sleeping mode, the power consumption of DSC n is expressed as $P_n^{SBS} = \frac{\frac{B}{10[\text{MHz}]}P_{BB}}{(1-\sigma_{DC})(1-\sigma_{MS})}$. The BB component is further turned off in the deep sleeping mode to reduce energy consumption while the small cell only remains base circuit power. The power consumption of deep sleeping DSC n is expressed as $P_n^{DES} = P_n^{SBS} - \frac{B}{10[\text{MHz}]}P_{BB}$.

According to the mobility prediction model in the P^{2}DM framework, some DSCs can be switched to the deep sleeping mode. The deep sleeping DSCs are added to the $\Phi_{sleeping}$ set. We assume that the number of deep sleeping DSCs is $|\Phi_{sleeping}|$. The total power consumption of the system P_{sum} can be expressed as

$$P_{sum} = (N - |\Phi_{sleeping}|)P_n^{ACT} + |\Phi_{sleeping}| P_n^{DES}. \quad (9)$$

F. ENERGY EFFICIENCY

The edge control center connects to the macro cell, which acts as a central controller to collect the information from all DSCs and perform complex computing tasks to set the operation parameters of DSCs. This paper aims to obtain a high downlink throughput with low energy consumption for the communication services of DSCs. Therefore, we define energy efficiency as the ratio of total system throughput Υ_{sum} to total power consumption P_{sum}, where the process of local calculation is not considered in the DSCs. The energy efficiency Ψ can be expressed as

$$\Psi = \frac{\Upsilon_{sum}}{P_{sum}} = \frac{\sum_{n}^{N}\sum_{k}^{K} B_{n,k} log_2(1+\zeta_{n,k})}{(N - |\Phi_{sleeping}|)P_n^{ACT} + |\Phi_{sleeping}| P_n^{\text{DES}}}. \quad (10)$$

IV. PREDICTION-BASED PROACTIVE DRONE MANAGEMENT (P^{2}DM) FRAMEWORK

Fig. 2 illustrates the process flows of the proposed P^{2}DM framework. It is shown that the framework consists of two major phases: offline training and online decision-making. A detailed description of these phases is provided in the following subsections.

A. OFFLINE TRAINING PHASE

In this subsection, we describe the procedures of the offline training phase.

- *Historical data*:
  Before the DSCs are temporarily dispatched for wireless networks, the macro cell's edge control center has been responsible for collecting past user' locations in the service area. In the past total T timeslots, the user position dataset is presented as $\mathbf{M} = \{M_k^1, M_k^2, \ldots, M_k^T\}$, called the historical user mobile data. The training data are

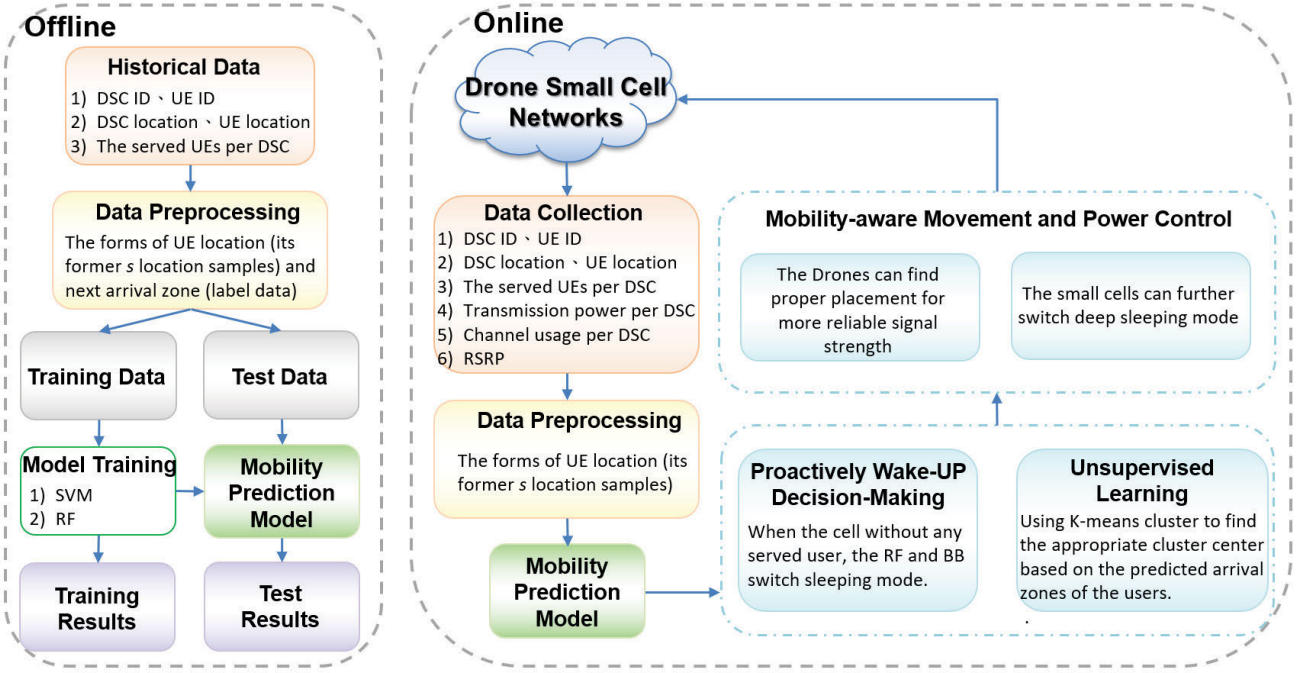

FIGURE 2. Process flow of the P^{2}DM framework.

obtained from the historical data to construct the mobile users' mobility prediction model.

- *Data preprocessing*:
  In the data preprocessing step, we can perform data transformation, formulation, or cleaning. Our mobility prediction model will infer the reached small grid g_k^{t+1} of user k at timeslot $t+1$, also called labeled data. The input data of the prediction model are set as the past continuous s samples set of user k at timeslot t, that is given by $\mathbf{X}_k^t = \{M_k^{t-s+1}, \ldots, M_k^{t-1}, M_k^t\}$. We assume that s value is far smaller than T (i.e., short-term location information). To prevent errors due to the diversity of the input data and labeled data, the positional data samples are normalized to the range $[-1, 1]$. The normalized samples are given by the following equation [14]:
  $$M_{k,nor}^t = 2 \cdot \frac{M_k^t - M_{min}}{M_{max} - M_{min}} - 1, \tag{11}$$
  where M_{max} and M_{min} are the maximum and minimum horizontal coordinates of the user in the rectangular service coverage area, respectively.
- *Training phase*:
  In our considered scenario, both the drones and users are mobile, leading to a highly dynamic and frequently changing network system. Therefore, it is not feasible to use long-term prediction methods. It is necessary to choose a suitable SL method for short-term predictions. To this end, we chose to use multi-class SVM and RF classifiers for training highly accurate prediction models. Seventy percent of the historical user mobile data is used as training data. Notably, one training data of the prediction model includes input data and label data, that is given by $\mathbf{T}_k^t = \{M_k^{t-s+1}, \ldots, M_k^{t-1}, M_k^t, g_k^{t+1}\}$. The prediction model is used to predict the user's arrival small grid at the next timeslot. Our system architecture has $N \times F \times F$ small grids (i.e., the number of classes in the mobility prediction model). In the simulation, we compare the accuracy of the prediction models trained by multi-class SVM and RF classifiers.
- *Testing phase*:
  The remainder of the historical user mobile data (i.e., 30%) is used as testing data to test the constructed prediction model. If a model is not sufficiently accurate, it is re-trained with updated training data (i.e., re-sampled 70% of the historical data) until a high accuracy in the testing step.

B. ONLINE DECISION-MAKING PHASE

In the online decision-making phase, the user position prediction model is used to make decisions. The procedures of the online decision-making phase are described below.

- *Data collection*:
  The edge control center of the macro cell is used to configure and collect the operational parameters. The network parameters include the users' and DSCs' identification numbers, position information, and the number of users in each DSC.
- *Data preprocessing*:
  The collected data are preprocessed, analyzed, and organized into a suitable form of input data for the prediction models to enable mobile users' location prediction.
- *Active waking/sleeping decisions*:
  According to the mobility prediction model, the reached small grid g_k^{t+1} of user k at the next timeslot $t+1$ can be

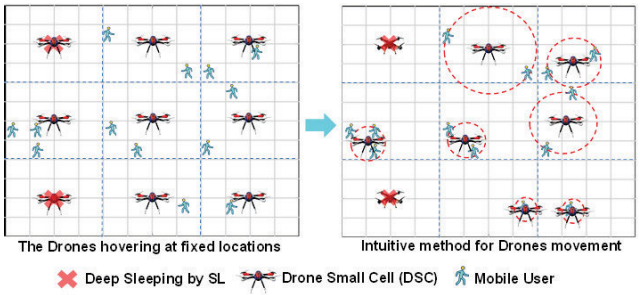

FIGURE 3. Fixed position and intuitive repositioning schemes.

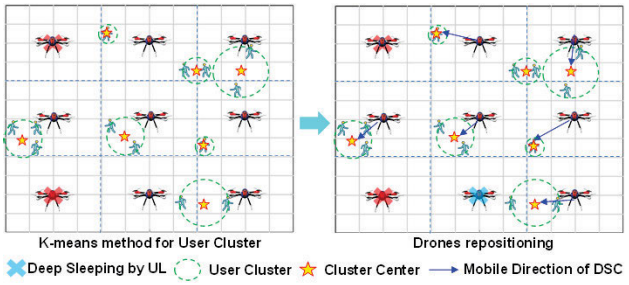

FIGURE 4. Illustration of UL repositioning.

predicted. When an active DSC is not serving any user, it can be switched to deep sleeping mode. We assume that each timeslot's length is longer than the awakening time from the deep sleep state. If g_k^{t+1} is located in the service coverage zone of a deep sleeping DSC, the control center proactively requires to wake up the deep sleeping DSC in timeslot t. This avoids the delay resulting from the awakening time and helps to save energy. Conversely, the DSC is passively woken after a user reaches its service coverage zone so that the QoS becomes instability.

- *UL repositioning mechanism*:
  The operation-state control of DSCs via the user mobility prediction model can significantly enhance energy efficiency. However, the interference construct in the DSC networks is changed when some of the DSCs are switched to sleeping mode. We use the UL technique to re-position DSCs and further perform power control to improve marginal users' throughput and the overall downlink reliability.

In the dynamic environment, the prediction model will be updated periodically for the online operation. The new user location information can be stored in the existing user position dataset at the online stage. In this way, the mobility prediction model needs to be renewed periodically based on the newest user position dataset.

V. UL REPOSITIONING MECHANISM

In this section, we describe the UL repositioning mechanism procedures in the P^{2}DM framework. In essence, this mechanism with the UL technique updates the positions of the DSCs and executes power control for interference mitigation and energy saving. Due to cost concerns in commercial applications, it is impractical to set up real DSC networks or perform detailed simulations for collecting the labeled data or rewards before providing communication services. The performance models are difficult to be built by data-driven SL or RL techniques. The UL techniques without any label data can find hidden structures by simply performing similarity analyses on the input data. Therefore, UL is suitable as a solution to improve energy efficiency in dynamic DSC networks.

The SL-based mobility prediction model is used to predict the reached small grid of each user at timeslot $t+1$, as shown on the left side of Fig. 3. The DSC is switched to the deep sleeping mode when the coverage zone has no served users. The DSCs in the left side of Fig. 3 are fixed at the center of their service coverage zones. However, it is possible to improve QoS by suitably repositioning the DSCs to shorten the DSC-to-user distances. The intuitive repositioning approach is illustrated on the right side of Fig. 3. The intuitive method for calculating the position of a drone at timeslot $t+1$ is as follows:

$$\begin{cases} D_n^{t+1}(x_n^{t+1}, y_n^{t+1}) = \dfrac{\sum_{k\in U_n}^{|U_n|} g_k^{t+1}(x_k^{t+1}, y_k^{t+1})}{|U_n|}, \\ \qquad \text{if } |U_n| \neq 0 \\ D_n^{t+1}(x_n^{t+1}, y_n^{t+1}) = D_n^t(x_n^t, y_n^t), \\ \qquad \text{if } |U_n| = 0 \end{cases} \tag{12}$$

where the $g_k^{t+1}(x_k^{t+1}, y_k^{t+1})$ is the central coordinates of the reached small grid of user k at timeslot $t+1$. In this intuitive scheme, the center location of $g_k^{t+1}, k \in U_n$ in the service coverage zone of DSC n is calculated. The DSCs are moved to their corresponding center locations to improve the QoS of the users. If an active DSC at timeslot t is switched to deep sleeping mode at the next timeslot $t+1$, the DSC hovers in the original position. We observe that the drones may come close to each other in the intuitive approach (e.g., in the bottom right corner of the Fig. 3), which leads to severe interference.

We propose a UL repositioning mechanism to address the interference problem. The KMC [43] is used to cluster users according to their predicted positions at timeslot $t+1$. Each DSC's reposition and power control is adjusted according to the clustering results within their limited range of flight to mitigate inter-DSC interference and reduce power consumption. The UL repositioning algorithm consists of two phases, as described below.

A. PHASE 1: DETERMINATION OF PUTATIVE DSC POSITIONS AND CANDIDATE RECOMMENDATION

In this stage, we use the KMC algorithm to cluster the predicted small grids of users at timeslot $t+1$, as shown on the left side of Fig. 4. Before performing the KMC algorithm, it is necessary to set the $\mathbf{K}$ value ($1 < \mathbf{K} \leq N$). $\left|\Phi_{active}^{t+1}\right|$ denotes the number of active DSCs, which is inferenced by the predicted small grids of users at timeslot $t+1$. Φ_{active}^{t+1} is the set of active DSCs at timeslot $t+1$. The $\mathbf{K}$ value is set

Algorithm 1 Unsupervised Learning (UL) Position Updating (Phase 1)

Phase 1: The Candidate DSCs of the Cluster Center.
$\left|\Phi_{active}^{t+1}\right|$ is # of the active DSCs at timeslot $t+1$.
K-means clustering is used to find the cluster center μ_i^{t+1} based on the predicted arrival grids of the users, where the presetting **K** is equal to $\left|\Phi_{active}^{t+1}\right|$, $1 \le i \le \mathbf{K}$.
The candidate DSC n of the cluster center μ_i^{t+1}, Φ_i^{t+1} is initialized to empty set.
for each DSC n of Φ_{active}^{t+1} **do**
  for each cluster i **do**
    $\min_i \left\| D_n^t(x_n^t, y_n^t) - \mu_i^{t+1}(x_i^{t+1}, y_i^{t+1}) \right\|$
  end for
  $n \rightarrow \Phi_i^{t+1}$, q becomes a member of Φ_i^{t+1}.
end for

to $\left|\Phi_{active}^{t+1}\right|$. The clustered objects are set to the predicted small grids of users at timeslot $t+1$. The horizontal coordinate of the object is the center position of the predicted small grid. The similarity matrix of the KMC algorithm is the Euclidean distance between a pair of objects. Two objects are close to each other, meaning that they have high similarity and vice versa. The KMC algorithm will place high similarity objects into the same cluster. Initial **K** cluster centers are selected randomly. Then the Euclidean distances between these centers and each object are calculated. Each object selects the closest cluster center as its center. If some objects select the same center, they are grouped into the same cluster. After the initial clusters have been formed, all objects' mean position in each cluster is calculated. This means the mean position will is set as the new cluster center. The objects are clustered iteratively by this procedure until the cluster centers satisfy the target function. The target function being minimized by the KMC algorithm is the squared Euclidean distance between the objects and their respective cluster centers:

$$\min \sum_{i=1}^{\mathrm{K}} \sum_{g_k^{t+1} \in C_i}^{|C_i|} \left\| g_k^{t+1}(x_k^{t+1}, y_k^{t+1}) - \mu_i^{t+1}(x_i^{t+1}, y_i^{t+1}) \right\|^2, \quad (13)$$

where μ_i^{t+1} is the cluster center of the i-th cluster, c_i. When the selected cluster centers are stable by iteration processes, the algorithm and the target function have been converged and minimized, respectively. Based on the cluster centers are determined by the KMC algorithm, the candidate new positions of all drones can be found at timeslot $t+1$.

Each DSC in the limited zone will try to choose the closest cluster center as its new position at timeslot $t+1$, which is

$$\min_i \left\| D_n^t(x_n^t, y_n^t) - \mu_i^{t+1}(x_i^{t+1}, y_i^{t+1}) \right\|. \quad (14)$$

According to (13), each DSC can choose its closest cluster center at timeslot $t+1$. Multiple DSCs may select the same cluster center. Therefore, a candidate DSC set is constructed for each cluster center (i.e., new position). Φ_i^{t+1} denotes the set of candidate drones for the i-th cluster center at timeslot $t+1$. We have described the first phase of the UL repositioning algorithm. The corresponding pseudocode is shown in Algorithm 1.

Algorithm 2 Unsupervised Learning (UL) Position Updating (Phase 2)

Phase 2: The Specified DSC of the Cluster Center.
$\left|\Phi_{active}^{t+1}\right|$ is # of the candidate DSCs of the μ_i^{t+1} at timeslot $t+1$.
for each cluster i **do**
  if $\left|\Phi_i^{t+1}\right| \ge 2$ **then**
    for each DSC $n \in \Phi_i^{t+1}$ **do**
      $\min_i \left\| D_n^t(x_n^t, y_n^t) - \mu_i^{t+1}(x_i^{t+1}, y_i^{t+1}) \right\|$
    end for
    Specified DSC $n \in \Phi_i^{t+1}$ can fly to the position of μ_i^{t+1}.
    Unspecified DSC $l \ne n, l \in \Phi_i^{t+1}$ switch deep sleeping its small cell.
  end if
  if $\left|\Phi_i^{t+1}\right| = 1$ **then**
    The DSC $l \ne n, l \in \Phi_i^{t+1}$ can fly to the position of μ_i^{t+1}.
  end if
  if $\left|\Phi_i^{t+1}\right| = [\ ]$ **then**
    No Drone fly to the position of μ_i^{t+1}.
  end if
end for

B. PHASE 2: DRONE SELECTION AND POWER-CONSUMPTION ADJUSTMENT

Each cluster center (i.e., the putative drone position) has a candidate drone set during the first phase. Suppose that $\left|\Phi_i^{t+1}\right|$ is the number of candidate drones in the candidate drone set of the i-th cluster center. There are three different decisions that could be made depending on the value of $\left|\Phi_i^{t+1}\right|$:

- $\left|\Phi_i^{t+1}\right| \ge 2$:
  This means that there are more than two candidate drones at cluster center i. The closest DSC $n \in \Phi_i^{t+1}$ is moved to the coordinates of cluster center i at timeslot $t+1$, according to the following expression:
  $$\min_n \left\| \mu_i^{t+1}(x_i^{t+1}, y_i^{t+1}) - D_n^t(x_n^t, y_n^t) \right\|, n \in \Phi_i^{t+1}. \quad (15)$$
  The other DSCs $l \ne n$ in Φ_i^{t+1} are switched to the deep sleeping mode for energy saving and interference reduction, as shown in the bottom right of Fig. 4.
- $\left|\Phi_i^{t+1}\right| = 1$:
  This means that there is only one candidate drone for the i-th cluster center. The closest DSC moves itself to the i-th cluster center at timeslot $t+1$.

TABLE 2. DSC system parameters.

Symbol	Quantity	Value
B	System bandwidth per carrier	10 MHz
ι_n	An DSC n with cell load	1 (Full-buffer)
τ_1, τ_2	Environmental parameter of air-to-ground channel model	9.61, 0.16
δ_{LoS}	Mean additional losses for LoS	1 dB
δ_{NLoS}	Mean additional losses for NLoS	20 dB
$P_{PA,max}$	PA maximum consumption	3.2 W
P_{RA}	Radio frequency base consumption	1.5 W
P_{BB}	BB base consumption	6.8 W
σ_{DC}	DC-DC conversion losses	6.4 %
σ_{MS}	Main supply losses	7.7 %
P_{max}^{tra}	Maximum transmit power per cell	30 dBm

- $\left|\Phi_i^{t+1}\right| = [\ ]$:
  This means that there are no candidate drones for the i-th cluster center. Therefore, this cluster center μ_i^{t+1} will not be set to the putative drone positions at timeslot $t+1$, as shown in the upper right of Fig. 4.

We have described the procedures of the second phase of the UL repositioning algorithm. The corresponding pseudocode is shown in Algorithm 2.

To summarize the discussion above, the first phase of the UL repositioning algorithm determines the putative drone positions and their corresponding set of candidate drones. In the second phase, drone repositioning and power adjustments are performed according to the clustering results. The object of the UL repositioning algorithm is to reduce interference and power consumption for DSC networks.

VI. SIMULATION RESULTS

In our considered scenario, we evaluate the performance of the proposed power control and positional updating in the P^{2}DM framework. Fig. 1 shows the simulation environment, where w and F are set to 40 m and 4, respectively. The simulated scenario has 9 DSCs ($N = 9$), and the altitude of the all drones are set to $h = 10$ m owing to user safety considerations [44]. The macro cell operates with $f_{BL} = 3.5$ GHz carrier frequency [45]. The DSC's data transmission frequency is set to $f_{AL} = 2$ GHz [46]. The DSC system parameters are listed in Table 2 [34], [38], [39], [47]. The system bandwidth $B = 10$ MHz of each DSC can be shared to served group users (i.e., each channel is fully loaded) [39]. In the air-to-ground channel model, we consider the urban scenario and its environmental parameters are $(\tau_1, \tau_2, \delta_{LoS}, \delta_{NLoS}) = (9.61, 0.16, 1, 20)$ given by [34], [47]. The PA maximum consumption is $P_{PA,max}$ & $= 3.2$ W, the radio frequency base consumption is $P_{RA} = 1.5$ W, and the BB base consumption is $P_{BB} = 6.8$ W. In the loss factors, the DC-DC conversion losses is $\sigma_{DC} = 6.4$ % and the main supply losses is $\sigma_{MS} = 7.7$ % [38]. Furthermore, maximum transmit power per cell is $P_{max}^{tra} = 30$ dBm [47]. In the user mobility model, the maximum shift angle θ_{max} is π. The historical user mobility data set contains about 36,000 location information. Besides, we evaluate the energy consumption of DSCs flight. When the drone's flying speed is lower than 8 m/sec, the drone's energy consumption is the same as the energy consumed by hovering [48]. We assume that the drone's flying speed is less than 8 m/sec, according to the user's maximum moving speed V_{max} is about 3 m/sec. Therefore, the low-speed mobile flight of the UAV will not generate additional energy consumption in our simulation.

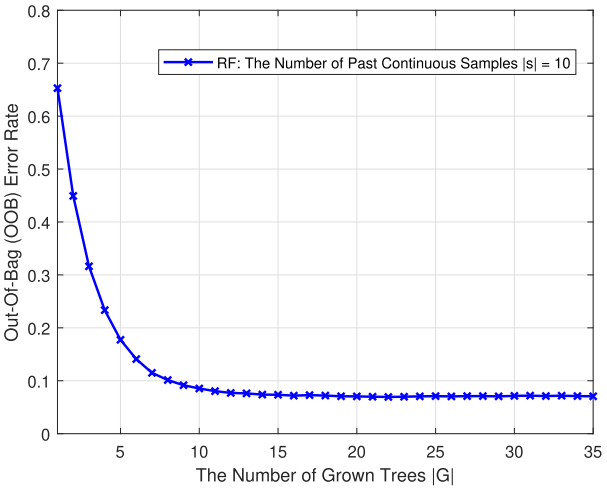

FIGURE 5. The out-of-bag error rate of random forest (RF) mobility prediction models.

A. COMPARISON OF SUPPORT VECTOR MACHINE (SVM) AND RANDOM FOREST (RF) MOBILITY PREDICTION MODELS

This section compares the performance of the mobility prediction models trained by the SVM and RF methods. The out-of-bag (OOB) error [49] is an error estimation technique, which is often used to evaluate the accuracy of a RF and to select appropriate values for tuning the number of the grown tree (i.e., predictors). It has been proved that OOB error estimation can be used as a generalization error to evaluate the classification ability of the classifier [50]. Fig. 5 shows the OOB of the RF mobility prediction model for different the number of grown trees.

From this figure, the following can be observed.

1) The OOB error estimation is an unbiased estimation of the RF algorithm. We can see that the error decreases concerning the number of grown trees increases.
2) When the number of grown trees |G| of 15 and above, the optimal OOB error rate is about 0.07.

Fig. 6 compares the accuracy of the mobility prediction models versus the number of past continuous samples $|s|$ when applying various supervised learning technologies: 1) prediction model trained by SVM; 2) prediction model trained by RF with the number of grown trees of 15; 3) prediction model trained by RF with the number of grown trees of 30. From this figure, the following can be observed.

1) In the SVM mobility prediction model, we observe that increasing the number of past continuous samples $|s|$ may clearly enhance the prediction accuracy due to the number of features (i.e., dimensions) growth. When the number of past continuous samples $|s|$ is 35,

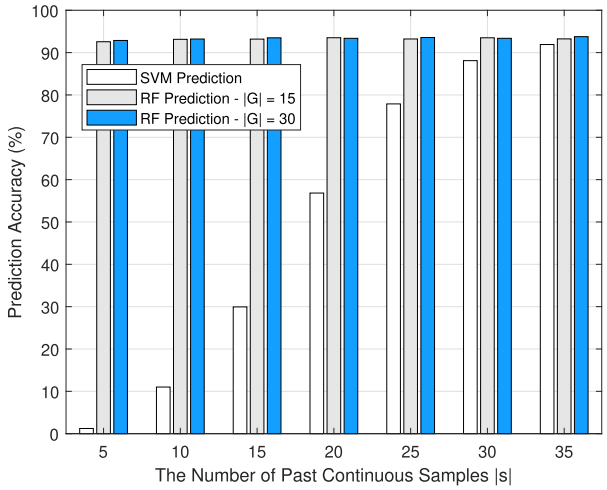

FIGURE 6. Comparison between the accuracy of support vector machine (SVM) and random forest (RF) mobility prediction models.

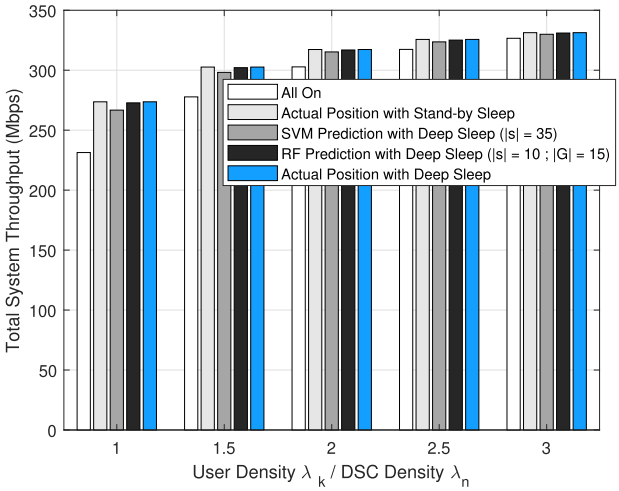

FIGURE 7. Improvements in total system throughput according to each power control scheme.

the prediction accuracy of the SVM model can achieve 91.91%. But high $|s|$ needs more execution time for training phase.

2) In the RF mobility prediction model, we first note that the number of grown trees $|G|$ of 15 and 30 have approximate accuracies. In addition, the accuracy of the RF mobility prediction model is slightly affected by the number of past continuous samples $|s|$. To accomplish the purpose, the RF builds a sufficient number of decision trees (i.e., 15 and above) and merges them to get a more accurate and stable prediction.
3) The RF mobility prediction model with $|G| = 15$ can run over the accuracy of 93.14% under the number of past continuous samples $|s| = 10$ and above. Therefore, the RF mobility prediction model with $|s| = 10$ and $|G| = 15$ can achieve high prediction accuracy while has relatively less execution time for training phase.

In the following, the benefits of RF and SVM prediction models combined with the deep sleeping mode compare with those of a few conventional operating schemes. In this comparison, the following schemes include: 1) The "all on" mode, where all of the DSCs are constantly active; 2) The DSC is switched to stand-by sleeping mode if there are no users to service in its service coverage zone; and 3) The DSC is switched to deep sleeping mode based on the actual positions of users at timeslot $t + 1$. Fig. 7 shows the total system throughput versus the ratio of user density λ_k to DSC density λ_n for various power control schemes. From the figure, we observe the following:

1) The stand-by and deep sleep states with actual positions have consistent performances because they have the same small cell on/off configuration in the system.
2) Under the deep sleep, the mobile user prediction by the SVM ($|s| = 35$) and RF ($|s| = 10$, $|G| = 15$) have approximate performance compared to the actual position of users.
3) Compared to the baseline scheme (i.e., all on), the deep sleep with RF prediction can improve total system throughput by 18.1% when the ratio is $\lambda_k/\lambda_n = 1$.

Fig. 8 shows the energy saving of each scheme versus the ratio of λ_k/λ_n for various power control schemes. From the figure, we have the following observation:

1) We first note that the deep sleeping mode saves considerably more energy than the stand-by sleeping mode. This is because the BB component is completely turned off in deep sleeping to reduce more energy consumption.
2) Secondly, this observation suggests that the energy saving of the deep sleep with RF prediction model ($|s| = 10$, $|G| = 15$) and the deep sleep with the actual position are very close.
3) The deep sleep with RF prediction model ($|s| = 10$, $|G| = 15$) can achieve 29.1% of energy saving over the baseline scheme when the ratio is $\lambda_k/\lambda_n = 1$.

B. EFFECT OF PREDICTION-BASED PROACTIVE DRONE MANAGEMENT (P^{2}DM) FRAMEWORK

In the previous section, the network performance of DSCs with fixed flying positions (i.e., the center of their service coverage zones) is evaluated. In this section, we compare the energy efficiency of repositioning schemes based on the RF mobility prediction model with deep sleeping mode. In this comparison, six schemes include: 1) The baseline "all on" scheme; 2) The "stand-by" sleeping scheme with the fixed central position in the service coverage zone; 3) The RF prediction-based deep sleeping with the fixed central position in the service coverage zone; 4) The RF prediction-based deep sleeping scheme combined with intuitive repositioning; 5) RF prediction-based deep sleeping scheme combined with K-means repositioning (i.e., the cluster centers are set as the new positions of DSCs); and 6) The proposed P^{2}DM framework. Fig. 9 illustrates how the energy efficiency of

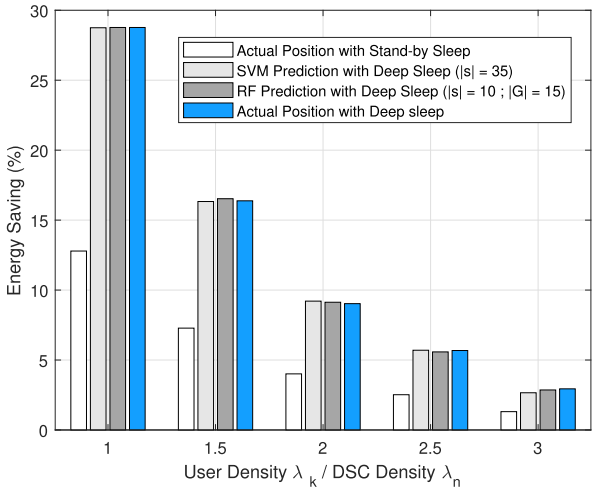

FIGURE 8. Energy saving of each power control scheme.

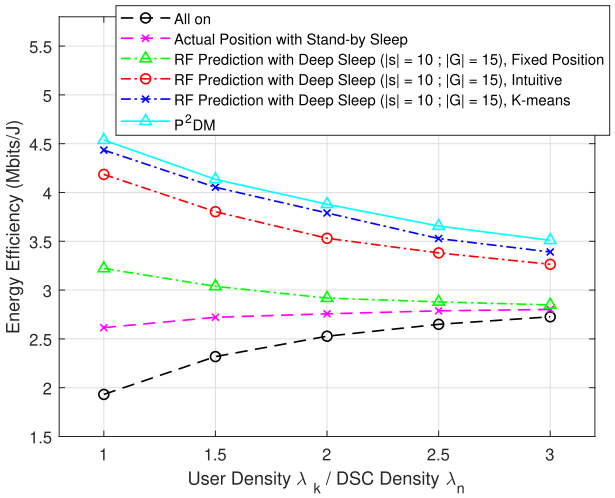

FIGURE 9. Comparison between the energy efficiency of power control and repositioning schemes.

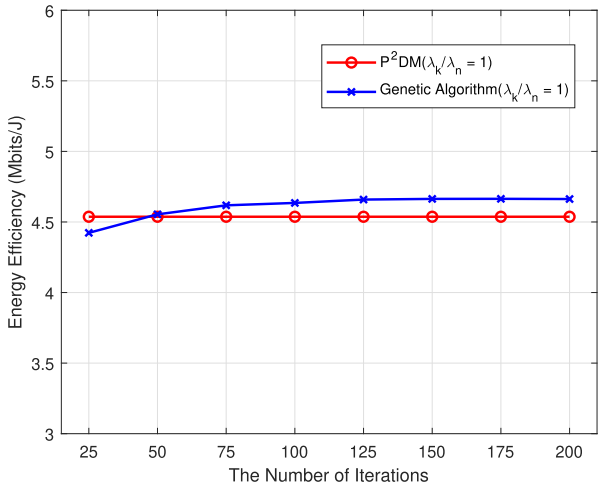

FIGURE 10. The energy efficiency of the P²DM framework and the genetic algorithm (GA) against the various number of iterations.

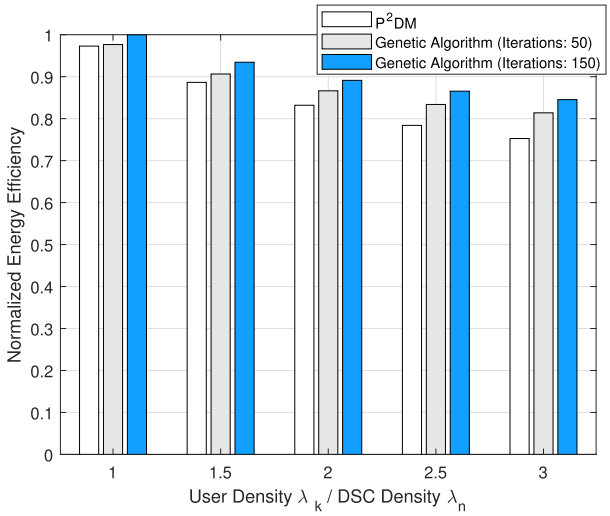

FIGURE 11. The normalized energy efficiency of the P²DM framework and the genetic algorithm (GA) against the ratio of λ_k/λ_n.

the DSC networks versus the ratio of λ_k/λ_n. In the figure, the following may be observed:

1) Compared to the baseline scheme (i.e., all on), the proposed P^{2}DM framework can improve energy efficiency by 133.9% when the ratio is $\lambda_k/\lambda_n = 1$.
2) Compared to the other all schemes, our P^{2}DM framework can significantly improve the energy efficiency when the high value of λ_k/λ_n.
3) Under the RF prediction-based deep sleeping scheme, the KMC scheme ranks second, which has higher energy efficiency than the intuitive method (i.e., the center of served users). The actual user position with stand-by sleeping performs worse than all the schemes except for the baseline scheme.

In addition, we further compare the normalized execution time and normalized energy efficiency of the proposed P^{2}DM framework with the optimal solution based on the genetic algorithm (GA) [51]. GA is a heuristic algorithm to find the optimum solution based on genetic and random selection [51]. The fitness value (i.e., the optimized solution) takes the value of the better fitted chromosome among all the chromosomes compared at each iteration. In light of this, we assume that the fitness value is set to the energy efficiency (i.e., KPI). Therefore, the energy efficiency of DSC networks needs to be calculated based on air to ground channel model at each iteration. Normally, GA uses a great number of iterations to provide a satisfactory solution. Fig. 10 shows the energy efficiency of the P^{2}DM framework and the GA against different the number of iterations $|I|$. In the GA, we first note that the number of iterations $|I|$ of 150 and above has approximate optimal energy efficiency. Therefore, the GA with $|I| = 150$ can achieve the optimal solution. Table 3 provides the normalized execution time of the proposed P^{2}DM framework to compare with the GA under $|I| = 50$ and 150. The normalized execution time is normalized to the longest execution time of the GA with $|I| = 150$. Our proposed P^{2}DM framework only spends 0.4% in terms of the execution time compared to the GA with $|I| = 150$ when the ratio is $\lambda_k/\lambda_n = 3$.

TABLE 3. The normalized execution time of the P^{2}DM framework and the genetic algorithm (GA) against the ratio of λ_k/λ_n.

The Ratio of User Density λ_k to DSC Density λ_n	Genetic Algorithm (Iterations: 150)	Genetic Algorithm (Iterations: 50)	Our Proposed P^{2}DM
$\lambda_k/\lambda_n = 1.0$	0.4141	0.1371	0.0037
$\lambda_k/\lambda_n = 1.5$	0.6042	0.1941	0.0041
$\lambda_k/\lambda_n = 2.0$	0.7386	0.2359	0.0043
$\lambda_k/\lambda_n = 2.5$	0.8644	0.2822	0.0044
$\lambda_k/\lambda_n = 3.0$	1.0000	0.3292	0.0046

We observe that P^{2}DM maintains about the same execution time as the ratio of λ_k/λ_n increases. The execution time of the GA grows dramatically as the ratio of λ_k/λ_n increases because the KPI needs to be calculated at each iteration. Fig. 11 shows the normalized energy efficiency of the two aforementioned algorithms against the ratio of λ_k/λ_n. The normalized energy efficiency is normalized to the maximum energy efficiency of the GA with $|I| = 150$. When the ratio is $\lambda_k/\lambda_n = 1$, P^{2}DM can achieve 97.3% of the energy efficiency over the GA with $|I| = 150$. In addition, P^{2}DM only drops 9% compared to the GA with $|I| = 150$ when the ratio is $\lambda_k/\lambda_n = 3$.

VII. CONCLUSION

Deploying flexible DSCs can provide service coverage and system throughput to respond to the scenario of hot spots or unforeseen natural disaster areas. In this paper, we establish a mobility prediction-based framework (i.e., the P^{2}DM framework) for DSCs management to improve energy efficiency and mitigate interference in the DSC-assisted wireless networks. The proposed P^{2}DM framework consists of offline and online phases. The RF-based mobility prediction model with high accuracy of 93.14% is built from a small sample data in the offline phase. In the online phase, the wake/sleeping schemes of the DSCs are proactively determined according to the predicted user positions. Then the UL technique is used to update the positions of the DSCs and to adjust their power consumption levels. We find through simulations that the proposed P^{2}DM framework can improve the energy efficiency by 133.9% compared to the baseline scheme. This study only addresses the interference and energy consumption problems of DSC-to-user access links. The edge computing and caching technologies in each DSC are the other two interesting future directions. The latency and computer energy efficiency trade-off in DSC networks is a ciritial issue in the case of limited-capacity backhaul links (i.e., macro cell-to-DSC links).

REFERENCES

[1] D. Liu, Y. Xu, J. Wang, J. Chen, K. Yao, Q. Wu, and A. Anpalagan, "Opportunistic UAV utilization in wireless networks: Motivations, applications, and challenges," *IEEE Commun. Mag.*, vol. 58, no. 5, pp. 62–68, May 2020.

[2] H. Hellaoui, A. Chelli, M. Bagaa, and T. Taleb, "Efficient steering mechanism for mobile network-enabled UAVs," in *Proc. IEEE Global Commun. Conf. (GLOBECOM)*, Waikoloa, HI, USA, Dec. 2019, pp. 1–6.

[3] O. Bekkouche, K. Samdanis, M. Bagaa, and T. Taleb, "A service-based architecture for enabling UAV enhanced network services," *IEEE Netw.*, vol. 34, no. 4, pp. 328–335, Jul. 2020.

[4] Q. Wu, J. Xu, Y. Zeng, D. W. K. Ng, N. Al-Dhahir, R. Schober, and A. L. Swindlehurst, "A comprehensive overview on 5G- and-beyond networks with UAVs: From communications to sensing and intelligence," 2020, *arXiv:2010.09317*. [Online]. Available: https://arxiv.org/abs/2010.09317

[5] A. A. Khuwaja, G. Zheng, Y. Chen, and W. Feng, "Optimum deployment of multiple UAVs for coverage area maximization in the presence of co-channel interference," *IEEE Access*, vol. 7, pp. 85203–85212, 2019.

[6] S. J. Nawaz, S. K. Sharma, S. Wyne, M. N. Patwary, and M. Asaduzzaman, "Quantum machine learning for 6G communication networks: State-of-the-art and vision for the future," *IEEE Access*, vol. 7, pp. 46317–46350, 2019.

[7] G. Zhu, D. Liu, Y. Du, C. You, J. Zhang, and K. Huang, "Toward an intelligent edge: Wireless communication meets machine learning," *IEEE Commun. Mag.*, vol. 58, no. 1, pp. 19–25, Jan. 2020.

[8] L.-C. Wang and S.-H. Cheng, "Self-organizing ultra-dense small cells in dynamic environments: A data-driven approach," *IEEE Syst. J.*, vol. 13, no. 2, pp. 1397–1408, Jun. 2019.

[9] L.-C. Wang and S.-H. Cheng, "Data-driven resource management for ultra-dense small cells: An affinity propagation clustering approach," *IEEE Trans. Netw. Sci. Eng.*, vol. 6, no. 3, pp. 267–279, Jul. 2019.

[10] S.-H. Cheng, Y.-S. Chao, L.-C. Wang, and A.-H. Tsai, "Affinity propagation clustering for interference management in aerial small cells," in *Proc. IEEE VTS Asia Pacific Wireless Commun. Symp. (APWCS)*, Singapore, Aug. 2019, pp. 1–5.

[11] L.-C. Wang, Y.-S. Chao, S.-H. Cheng, and Z. Han, "An integrated affinity propagation and machine learning approach for interference management in drone base stations," *IEEE Trans. Cognit. Commun. Netw.*, vol. 6, no. 1, pp. 83–94, Mar. 2020.

[12] A. Iqbal, M.-L. Tham, and Y. C. Chang, "Double deep Q-network for power allocation in cloud radio access network," in *Proc. IEEE 3rd Int. Conf. Comput. Commun. Eng. Technol. (CCET)*, Aug. 2020, pp. 272–277.

[13] A. Iqbal, M.-L. Tham, and Y. C. Chang, "Double deep Q-network-based energy-efficient resource allocation in cloud radio access network," *IEEE Access*, vol. 9, pp. 20440–20449, 2021.

[14] J. Yang, C. Dai, and Z. Ding, "A scheme of terminal mobility prediction of ultra dense network based on SVM," in *Proc. IEEE 2nd Int. Conf. Big Data Anal. (ICBDA)*, Beijing, China, Mar. 2017, pp. 837–842.

[15] S. Tian, X. Zhang, Y. Zhang, Z. Cao, and W. Cao, "Spatio-temporal position prediction model for mobile users based on LSTM," in *Proc. IEEE 25th Int. Conf. Parallel Distrib. Syst. (ICPADS)*, Tianjin, China, Dec. 2019, pp. 967–970.

[16] W. Yuan, C. Liu, F. Liu, S. Li, and D. W. K. Ng, "Learning-based predictive beamforming for UAV communications with jittering," *IEEE Wireless Commun. Lett.*, vol. 9, no. 11, pp. 1970–1974, Nov. 2020.

[17] X. Liu, J. Yu, H. Qi, J. Yang, W. Rong, X. Zhang, and Y. Gao, "Learning to predict the mobility of users in mobile mmWave networks," *IEEE Wireless Commun.*, vol. 27, no. 1, pp. 124–131, Feb. 2020.

[18] M. Fernández-Delgado, E. Cernadas, S. Barro, and D. Amorim, "Do we need hundreds of classifiers to solve real world classification problems?" *J. Mach. Learn. Res.*, vol. 15, no. 1, pp. 3133–3181, 2014.

[19] X. Liu, Y. Liu, and Y. Chen, "Reinforcement learning in multiple-UAV networks: Deployment and movement design," *IEEE Trans. Veh. Technol.*, vol. 68, no. 8, pp. 8036–8049, Aug. 2019.

[20] S. K. Singh, K. Agrawal, K. Singh, C.-P. Li, and W.-J. Huang, "On UAV selection and position-based throughput maximization in multi-UAV relaying networks," *IEEE Access*, vol. 8, pp. 144039–144050, 2020.

[21] J. Guo, Y. Huo, X. Shi, J. Wu, P. Yu, L. Feng, and W. Li, "3D aerial vehicle base station (UAV-BS) position planning based on deep Q-learning for capacity enhancement of users with different QoS requirements," in *Proc. 15th Int. Wireless Commun. Mobile Comput. Conf. (IWCMC)*, Tangier, Morocco, Jun. 2019, pp. 1508–1512.

[22] Z. Kang, C. You, and R. Zhang, "3D placement for multi-UAV relaying: An iterative gibbs-sampling and block coordinate descent optimization approach," *IEEE Trans. Commun.*, vol. 69, no. 3, pp. 2047–2062, Mar. 2021, doi: 10.1109/TCOMM.2020.3043776.

[23] Q. Chen, "Joint position and resource optimization for multi-UAV-aided relaying systems," *IEEE Access*, vol. 8, pp. 10403–10415, 2020.

[24] C. Liu, B. Natarajan, and H. Xia, "Small cell base station sleep strategies for energy efficiency," *IEEE Trans. Veh. Technol.*, vol. 65, no. 3, pp. 1652–1661, Mar. 2016.

[25] G. Jang, N. Kim, T. Ha, C. Lee, and S. Cho, "Base station switching and sleep mode optimization with LSTM-based user prediction," *IEEE Access*, vol. 8, pp. 222711–222723, 2020.

[26] H. Yang and X. Xie, "Energy-efficient joint scheduling and resource management for UAV-enabled multicell networks," *IEEE Syst. J.*, vol. 14, no. 1, pp. 363–374, Mar. 2020.
[27] X. Liu, Y. Liu, Y. Chen, and L. Hanzo, "Trajectory design and power control for multi-UAV assisted wireless networks: A machine learning approach," *IEEE Trans. Veh. Technol.*, vol. 68, no. 8, pp. 7957–7969, Aug. 2019.
[28] F. Zhou and R. Q. Hu, "Computation efficiency maximization in wireless-powered mobile edge computing networks," *IEEE Trans. Wireless Commun.*, vol. 19, no. 5, pp. 3170–3184, May 2020.
[29] X. Zhang, Y. Zhong, P. Liu, F. Zhou, and Y. Wang, "Resource allocation for a UAV-enabled mobile-edge computing system: Computation efficiency maximization," *IEEE Access*, vol. 7, pp. 113345–113354, 2019.
[30] C. Y. Aung, B. C. Seet, M. Zhang, L. F. Xie, and P. H. J. Chong, "A review of group mobility models for mobile ad hoc networks," *Wireless Pers. Commun.*, vol. 85, no. 3, pp. 1317–1331, 2015.
[31] F. Geng and S. Xue, "A comparative study of mobility models in the performance evaluation of MCL," in *Proc. 22nd Wireless Opt. Commun. Conf.*, Chongqing, China, May 2013, pp. 288–292.
[32] G. Jayakumar and G. Ganapathi, "Reference point group mobility and random waypoint models in performance evaluation of MANET routing protocols," *J. Comput. Syst., Netw., Commun.*, vol. 2008, pp. 1–10, Dec. 2008.
[33] M. Mozaffari, W. Saad, M. Bennis, and M. Debbah, "Drone small cells in the clouds: Design, deployment and performance analysis," in *Proc. IEEE Global Commun. Conf. (GLOBECOM)*, San Diego, CA, Dec. 2015, pp. 1–6.
[34] A. Al-Hourani, S. Kandeepan, and S. Lardner, "Optimal LAP altitude for maximum coverage," *IEEE Wireless Commun. Lett.*, vol. 3, no. 6, pp. 569–572, Dec. 2014.
[35] M. Youssef, C. A. Nour, J. Farah, and C. Douillard, "Backhaul-constrained resource allocation and 3D placement for UAV-enabled networks," in *Proc. IEEE 90th Veh. Technol. Conf. (VTC-Fall)*, Honolulu, HI, USA, Sep. 2019, pp. 1–7.
[36] G. Auer, V. Giannini, C. Desset, I. Godor, P. Skillermark, M. Olsson, M. A. Imran, D. Sabella, M. J. Gonzalez, O. Blume, and A. Fehske, "How much energy is needed to run a wireless network?" *IEEE Trans. Wireless Commun.*, vol. 18, no. 5, pp. 40–49, Oct. 2011.
[37] H. Holtkamp, G. Auer, V. Giannini, and H. Haas, "A parameterized base station power model," *IEEE Commun. Lett.*, vol. 17, no. 11, pp. 2033–2035, Nov. 2013.
[38] D. Sabella, D. D. Antonio, K. Efstathios, I. M. Ali, D. G. Marco, S. Umer, L. Massinissa, S. Konstantinos, and M. Andreas, "Energy efficiency benefits of RAN-as-a-service concept for a cloud-based 5G mobile network infrastructure," *IEEE Access*, vol. 2, pp. 1586–1597, 2014.
[39] *Further Advancements for E-UTRA Physical Layer Aspects*, document TR 36.814 V9.0.0, 3GPP, Mar. 2010.
[40] M. Feng, S. Mao, and T. Jiang, "Base station ON-OFF switching in 5G wireless networks: Approaches and challenges," *IEEE Wireless Commun.*, vol. 24, no. 4, pp. 46–54, Aug. 2017.
[41] S. Rostami, K. Heiska, O. Puchko, K. Leppanen, and M. Valkama, "Novel wake-up scheme for energy-efficient low-latency mobile devices in 5G networks," *IEEE Trans. Mobile Comput.*, vol. 20, no. 4, pp. 1511–1528, Apr. 2021, doi: 10.1109/TMC.2020.2964218.
[42] K. P. Sinaga and M.-S. Yang, "Unsupervised K-means clustering algorithm," *IEEE Access*, vol. 8, pp. 80716–80727, 2020.
[43] S. Falangitis, P. Spapis, P. Magdalinos, G. Beinas, and N. Alonistioti, "Clustering for small cells," in *Proc. Eur. Conf. Netw. Commun. (EuCNC)*, 2014, pp. 1–5.
[44] Z. Becvar, M. Vondra, P. Mach, J. Plachy, and D. Gesbert, "Performance of mobile networks with UAVs: Can flying base stations substitute ultra-dense small cells?" in *Proc. 23th Eur. Wireless Conf.*, Dresden, Germany, May 2017, pp. 1–7.
[45] R. N. Esa, A. Hikmaturokhman, and A. R. Danisya, "5G NR planning at frequency 3.5 GHz: Study case in Indonesia industrial area," in *Proc. 2nd Int. Conf. Ind. Electr. Electron. (ICIEE)*, Lombok, Indonesia, Oct. 2020, pp. 187–193.
[46] *Study on Channel Model for Frequencies from 0.5 to 100 GHz*, document TR 38.901 version 14.0.0 Release 14, 3GPP, ETSI, 2017.
[47] A. Akarsu and T. Girici, "Resilient deployment of drone base stations," in *Proc. Int. Symp. Netw., Comput. Commun. (ISNCC)*, Istanbul, Turkey, Jun. 2019, pp. 1–5.
[48] A. Fotouhi, M. Ding, and M. Hassan, "DroneCells: Improving spectral efficiency using drone-mounted flying base stations," *J. Netw. Comput. Appl.*, vol. 174, Jan. 2021, Art. no. 102895.
[49] L. Breiman, "Random forests," *Mach. Learn.*, vol. 45, no. 1, p. 532, 2001, doi: 10.1023/A:1010933404324.
[50] R. Wang, H. Wang, and L. Wang, "Feature selection of complex power quality disturbances and parameter optimization of random forest," in *Proc. 4th Int. Conf. Intell. Green Building Smart Grid (IGBSG)*, Hubei, Yi-Chang, China, Sep. 2019, pp. 384–387.
[51] R. Shivgan and Z. Dong, "Energy-efficient drone coverage path planning using genetic algorithm," in *Proc. IEEE 21st Int. Conf. High Perform. Switching Routing (HPSR)*, Newark, NJ, USA, May 2020, pp. 1–6.

SHAO-HUNG CHENG (Member, IEEE) received the B.S. and M.S. degrees from the Department of Applied Physics, Chung Cheng Institute of Technology (CCIT), National Defense University, Taiwan, in 2005 and 2008, respectively, and the Ph.D. degree from the Department of Electrical and Computer Engineering, National Chiao Tung University, Taiwan, in 2018. From 2013 to 2014, he was a Lecturer with the Department of Electrical and Electronic Engineering, CCIT, National Defense University. Since September 2018, he has been with CCIT. He is currently an Assistant Professor with the Department of Electrical and Electronic Engineering, National Defense University. His research interests include UAV communication, radio resource management in small cell networks, self-optimization, and machine learning.

YEN-TING SHIH was born in Taichung, Taiwan, in 1992. He received the B.S. degree from the Department of Electrical and Electronic Engineering, Chung Cheng Institute of Technology, National Defense University, Taoyuan, Taiwan, in 2016, where he is currently pursuing the M.S. degree with the Institute of Electrical and Computer Engineering. His current research interests include UAV resource management, wireless communication, and machine learning applications.

KO-CHIN CHANG (Member, IEEE) received the Ph.D. degree in electronic engineering from Chung Cheng Institute of Technology (CCIT), National Defense University, Taiwan, in 2010. Since 2011, he has been with the Department of Electrical Engineering, CCIT, where he is currently an Associate Professor with the Department of Electrical and Electronic Engineering. His research interests include penetration testing, information security, image and signal processing, data hiding, and image compression. His recent research has focused on information security.